PERGAMON

International Journal of Multiphase Flow 27 (2001) 1451–1461

International Journal of Multiphase Flow

www.elsevier.com/locate/ijmulflow

Flow across structured fiber bundles: a dimensionless correlation

T.D. Papathanasiou *

Department of Chemical Engineering, Swearingen Engineering Center, University of South Carolina, Columbia, SC 29208, USA

Received 31 January 2000; received in revised form 23 January 2001

Abstract

We present a computational analysis of viscous flow across unidirectional arrays of fiber bundles using the boundary element method (BEM). We consider hexagonal arrays of fiber bundles in which the individual filaments are packed in hexagonal or square arrangements. Up to 300 individual filaments are included in each simulation. These are simple but not trivial models for dual porosity fibrous media (such as the preforms used in composites manufacturing or fiber bundles used in hollow membrane oxygenators) characterized by different inter- and intra-tow porosities. The way these porosities interact to determine the hydraulic permeability of such media is not well understood. Numerical solution of the flow problem yields the flowrate through the unit cell, from which the hydraulic permeability (K_p) of the dual porosity medium is computed. Through a large number of simulations we determine K_p for a range of inter- and intra-tow porosities and for a range of fiber sizes. A semi-empirical correlation is proposed which collapses all the numerical data (a total of 380 data points) on a single curve, for both, hexagonal and square intra-tow fiber arrangements. This correlation allows prediction of the permeability of hexagonal arrays of fiber bundles from a knowledge of their inter- and intra-tow porosities, the type of intra-tow packing and the size (or number) of the intra-tow filaments.

1. Introduction

Fibrous porous media are usually idealized as made up of cylinders arranged in space in a defined periodic order. In such arrangements, a unit cell can be identified and its permeability calculated by solution of the pertinent flow equations, usually in the limits of small and large porosities (Bruschke and Advani, 1993; Sangani and Acrivos, 1982; Gebart, 1992; Drummond and Tahir, 1984;

* Tel.: +1-803-777-7219.
E-mail address: papathan@engr.sc.edu (T.D. Papathanasiou).

0301-9322/01/$ - see front matter
PII: S0301-9322(01)00013-1

Nagelhout et al., 1995). However, there are several cases in engineering, in which fibers are used in the form of bundles rather than as individual filaments. A notable example is the case of the fibrous preforms used in composites fabrication. In such preforms fibers are typically bundled together in tows, separated by fairly large gaps which facilitate resin flow during the saturation process. The porosity of these tows is invariably different from the "macroscopic" porosity of the system. Arrays of fiber bundles are classical dual-porosity media, characterized by their inter- (gaps between tows) and intra-tow (void space within a tow) porosities. The manner in which these interact to determine the flow through and the permeability of such fibrous media is not well understood, even though several studies have dealt theoretically with this problem (Parnas and Phelan, 1991; Pillai and Advani, 1995; Phelan and Wise, 1996; Ranganathan et al., 1996). In earlier work (Papathanasiou, 1996, 1997) we had presented the results of a computational study of Stokes flow across square arrays of fiber clusters containing relatively small number of filaments. Each cluster was made up of uniform fibers arranged in square packing. The hydraulic permeability of these systems was calculated from Darcy's Law (Darcy, 1856) following the numerical solution of Stokes' equations in the corresponding unit cell. It was found that the numerically computed permeabilities followed a correlation of the form $K_p/K_s - 1 = \alpha\chi^\beta$, where ($\chi$) is an effective intra-tow porosity ($\chi = 1 - (1 - \phi_t)/(1 - \phi_{max})$). α, β were found to be functions of the inter-tow porosity.

The main limitation of this study was the small number of fibers considered in each simulation and the fact that the effect of the fiber size was not investigated. Furthermore, a square arrangement of tows and of intra-tow fibers is not very realistic, as fibers and tows tend to assume positions closer to hexagonal packing as a result of external or hydrodynamic forces. The present communication extends these computations to hexagonal packing of the bundles (tows) and of the intra-tow fibers. The arrangements studied are indicated as hex–hex (HH) and hex–square (HS) (the first part of these terms corresponds to the inter- and the second to the intra-tow packing; for example, Fig. 1(a) refers to the HS unit cell). Much larger number of fibers (up to 300 in each bundle) have been considered in this study and therefore the computed permeabilities are not significantly affected by the shape of the tow-fluid interface (which, for the square packing of tows and the small fiber numbers used in earlier work (Papathanasiou, 1997) can be a problem at lower ϕ_i). The effect of the number of fibers making up each bundle is further illustrated. The principal advantage of this approach is that the structure of the interior of a tow is explicitly included in the simulation and reflected in the computed permeabilities; no assumption needs to be made about tow homogeneity, tow permeability or about the nature of the flow in the interior of the tow and at the tow/fluid interface. Our objective is to derive quantitative relations between primary, measurable variables (such as inter- and intra-tow porosities and the size (or number) of fibers making up each tow) and the permeability of such arrays of fiber bundles. The computational results are presented in a form deduced from the theoretical work of Ranganathan et al. (1996). Based on this representation we construct a master curve for the permeability of hexagonal arrays of fiber bundles for square and hexagonal intra-tow packing.

2. Model systems

We consider systems made up of infinitely long cylindrical bundles arranged in an hexagonal packing and with their axes perpendicular to the direction of flow. Each bundle consists of a

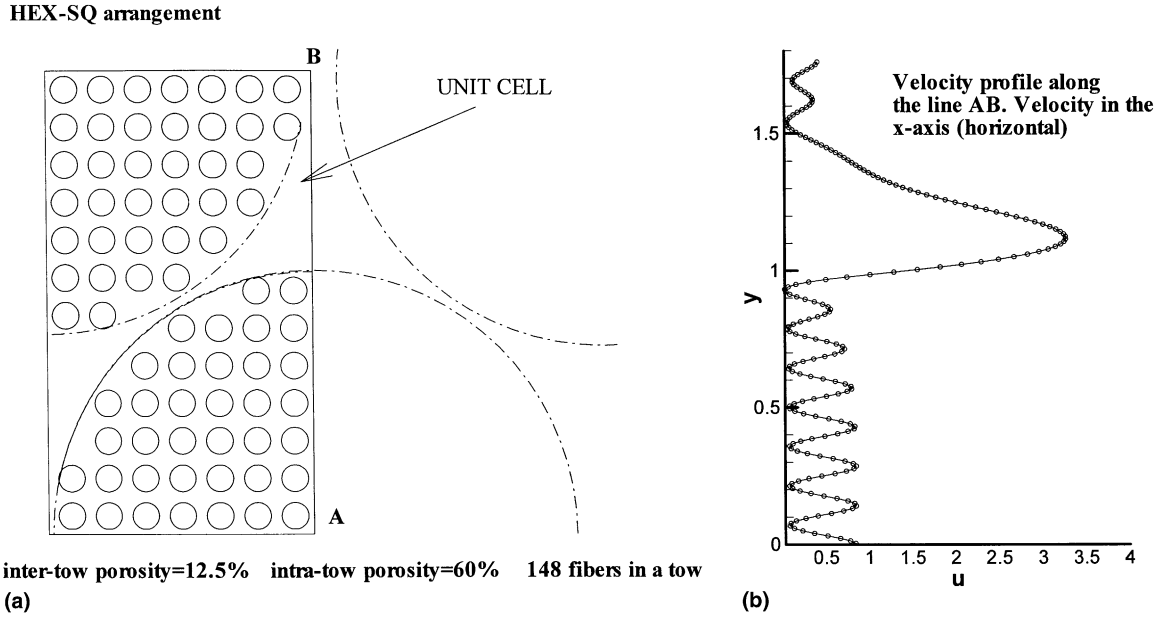

Fig. 1. The unit cell used in the HS arrangement. (a) Hexagonal packing of tows and square intra-tow packing of filaments. (b) Typical velocity profile along the line (AB).

number (N_f) of solid cylindrical filaments of radius R_f. These filaments are arranged in square or hexagonal packing within the bundle. Figs. 1 and 2 show typical unit cells corresponding to the two types of packing. We investigate the regions of small-to-moderate values of inter-tow (ϕ_i) and moderate-to-high values of intra-tow (ϕ_t) porosities (at low values of ϕ_t practically no fluid passes through the bundle which behaves effectively as an impermeable entity).

It is obvious that the overall permeability (K_p) of such a dual porosity system will be determined by the amount of fluid passing through the inter- and intra-tow regions. The latter is related to the permeability of the tow itself (K_{tow}, a function of ϕ_t) while the former should be related to the permeability of a system with the same inter-tow porosity but made up of impermeable tows. The permeability of this system is indicated as (K_s) and is only a function of ϕ_i. These unit cells are fully characterized when the type of inter- and intra-tow packing, as well as the inter- and intra-tow porosities (ϕ_i and ϕ_t) and either R_f or N_f are known. The intra-tow porosity and either R_f or N_f are the geometrical parameters that determine (K_{tow}). (K_s) is determined by the inter-tow porosity and the tow radius (R_t).

In any unit cell the permeability can be calculated from the flowrate (Q) through the cell (obtained by integration of the velocity profile along the inlet or outlet boundaries) and the corresponding pressure drop (ΔP), using Darcy's law $K = (Q/H)(L\mu/\Delta P)$. (H) and (L) are the height and length of the unit cell. The velocity profile is obtained by solving the pertinent flow problem (Stokes flow in our case). We use the boundary element method (BEM) for this purpose. Use of the BEM in solving Stokes flow problems is well documented (Brebbia and Dominquez, 1992). In brief, the equations solved are the Stokes equations for two-dimensional flow:

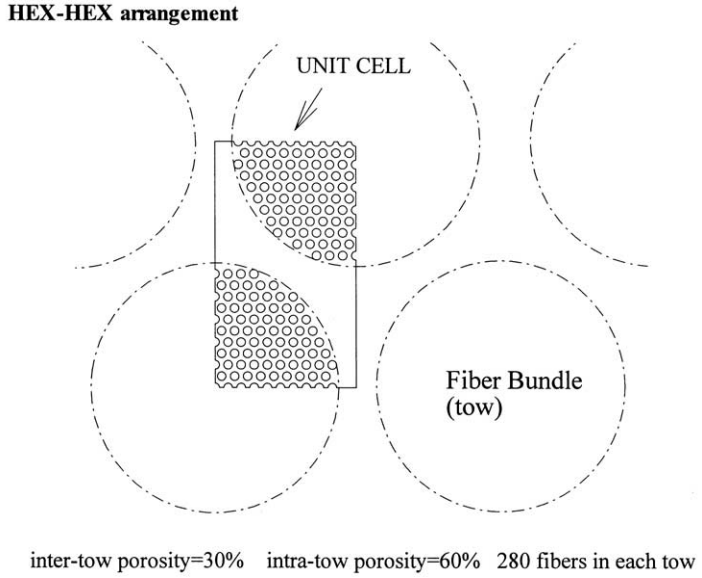

Fig. 2. The geometry and unit cell corresponding to the HH arrangement. Hexagonal packing of tows and hexagonal intra-tow packing of filaments.

$$\mu\left(\frac{\partial^2 u}{\partial x^2}+\frac{\partial^2 u}{\partial y^2}\right)=\frac{\partial P}{\partial x} \quad \text{and} \quad \mu\left(\frac{\partial^2 v}{\partial x^2}+\frac{\partial^2 v}{\partial y^2}\right)=\frac{\partial P}{\partial y} \quad \text{(momentum)}, \tag{1}$$

$$\frac{\partial u}{\partial x}+\frac{\partial v}{\partial y}=0 \quad \text{(continuity)}, \tag{2}$$

where (u) and (v) are the components of the velocity vector in the (x) and (y) directions, respectively, of the Cartesian coordinate system. The boundary conditions are: no-slip ($u=v=0$) conditions on the surface of the fibers, prescribed pressure drop between the inflow and outflow boundaries in the direction of bulk flow, and symmetry conditions on the fluid segments of the upper and lower boundaries. The numerical algorithm was coded to run on a 4-CPU server; this offered approximately a 2-time speedup as compared to running on a conventional single processor PC. An example of the velocity profile obtained in the HS arrangement is shown in Fig. 1(b). Even though as a result of the boundary conditions specifying the unit cell the velocity profile on the inflow and outflow boundaries is one-dimensional, the problem solved is a two-dimensional one and the complete flow distribution in the interior of the flow domain can be readily obtained from the boundary solution using Somigliana's identity (Brebbia and Dominquez, 1992).

3. Results and discussion

3.1. The permeability of hex–hex (HH) and hex–square (HS) arrays

A large number of simulations were carried out in HH and HS unit cells (Figs. 1 and 2). The parameters which varied were the inter-tow porosity (ϕ_i), the intra-tow porosity (ϕ_t) and the fiber

radius (R_f). The results are plotted in terms of the intrinsic permeability ($K_{in} = K_p/K_s - 1$) vs. the effective intra-tow porosity (χ)

$$\chi = 1 - (1 - \phi_t)/(1 - \phi_{max}) \tag{3}$$

in Figs. 3 and 4. A total of 231 data points are included in Fig. 3, corresponding to $\phi_i = 0.10, 0.12, 0.125, 0.15, 0.20$ and 0.30. ϕ_t is 0.50, 0.55, 0.6, 0.65, 0.70, 0.75, 0.8, 0.85, 0.9. The results from the

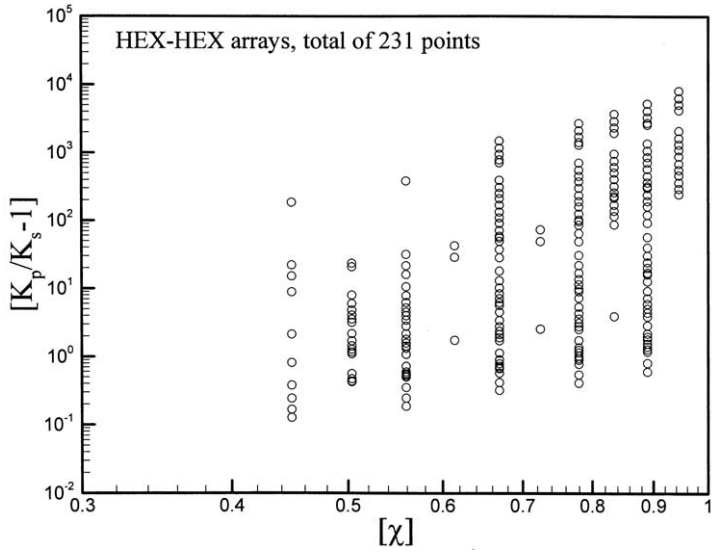

Fig. 3. Numerical results for the intrinsic permeability ($K_{in} = K_p/K_s - 1$) of HH arrays plotted on a log-log scale against the effective intra-tow porosity (χ) ($\chi = (1 - \phi_t)/(1 - \phi_{max})$).

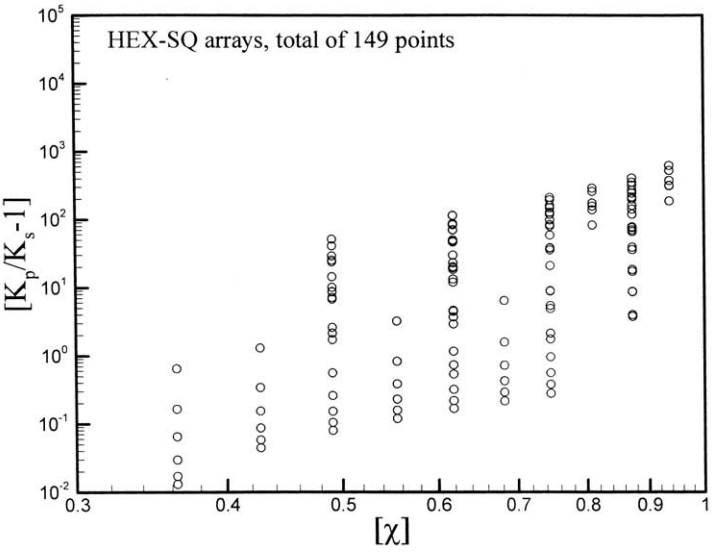

Fig. 4. Numerical results for the intrinsic permeability ($K_{in} = K_p/K_s - 1$) of HS arrays plotted on a log–log scale against the effective intra-tow porosity (χ) ($\chi = (1 - \phi_t)/(1 - \phi_{max})$).

HS arrays are shown in Fig. 4. In this case a total of 149 data points were obtained, corresponding to $\phi_i = 0.115$, 0.12, 0.125, 0.15, 0.20,0.3,0.35 and 0.40. ϕ_t is 0.50, 0.55, 0.6, 0.65, 0.70, 0.75, 0.8, 0.85, 0.9 and 0.95. The reader will notice that the number of data points at each level of (χ) in Figs. 3 and 4 is greater than the number of inter-tow porosities considered. This is because at each level of intra-tow porosity the number of fibers (N_f) in the tow is also varied along with ϕ_i. Increasing N_f at a fixed R_{tow} and ϕ_t reduces R_f and consequently reduces the tow permeability. Even though, as in Papathanasiou, 1997, the intrinsic permeabilities corresponding to the same ϕ_i and same R_f fall on approximately straight lines when plotted on a log–log scale against χ, the fact that the fiber radius (or tow permeability) is introduced as an additional parameter makes this not a very useful way to generalize our results. Since the inter-tow packing is hexagonal in both cases (Figs. 3 and 4), the differences in permeability observed between the two figures at the same level of χ and R_f are solely due to the difference in intra-tow packing.

3.2. A dimensionless correlation

It was argued earlier that the overall permeability (K_p) of a dual porosity system should be affected by the flow through the inter- as well as through the intra-tow spaces. The latter is related to the permeability of the tow itself (K_{tow}) while the former will be related to the permeability of a system with the same inter-tow porosity but made up of impermeable tows (K_s). Earlier studies (Papathanasiou, 1997; Sadiq et al., 1995) investigated expressions of the general form $K_p = f(K_{tow}, K_s)$. We pursue the same line of inquiry in this work because of the value of such a general correlation in design. The work of Ranganathan et al. (1996) suggests that the appropriate power of K_{tow} in such a correlation is (3/2). To produce a dimensionless group from the ratio $K_p/(K_{tow})^{3/2}$ it seems reasonable to multiply by $K_s^{1/2}$. The dimensionless group then becomes $K_p K_s^{1/2}/(K_{tow})^{3/2}$. Since in a dual porosity unit cell the ratio of the flow through the inter-tow to that through the intra-tow space is related to (K_s/K_{tow}), we express $K_p K_s^{1/2}/(K_{tow})^{3/2}$ as a polynomial of (K_s/K_{tow}). A possible correlation will therefore be of the form

$$\frac{K_p K_s^{1/2}}{K_{tow}^{3/2}} = f\left(\frac{K_s}{K_{tow}}\right). \tag{4}$$

In (4), K_{tow} and K_s can be calculated from the appropriate expressions (e.g. Gebart, 1992; Bruschke and Advani, 1993) and are therefore functions of ϕ_i, ϕ_t, R_t and R_f and of the type of packing, all measurable physical quantities. Plotting the BEM results for (K_p) as suggested by (4) results in a curve characterized by two power-law regions in the limit of large and small (K_s/K_{tow}). This suggests

$$f\left(\frac{K_s}{K_{tow}}\right) = a\left(\frac{K_s}{K_{tow}}\right)^n + \beta\left(\frac{K_s}{K_{tow}}\right)^m \text{ or } \frac{K_p K_s^{1/2}}{K_{tow}^{3/2}} = a\left(\frac{K_s}{K_{tow}}\right)^n \left(1 + \frac{\beta}{\alpha}\left(\frac{K_s}{K_{tow}}\right)^{m-n}\right). \tag{5}$$

Rearranging, we get

$$K_p = a\,\frac{(K_s)^{n-0.5}}{(K_{tow})^{n-1.5}}\left(1 + \frac{\beta}{\alpha}\left(\frac{K_s}{K_{tow}}\right)^{m-n}\right). \tag{6}$$

This is an empirical model with four adjustable parameters (α, β, n, m). This number can be reduced to two by observing that as (K_{tow}/K_s) approaches zero the permeability of the unit cell (K_p) should approach (K_s). In this case, the right-hand side of (6) becomes $((K_s)^{m-0.5}/(K_{tow})^{m-1.5})\beta$. For this to equal K_s, it must be: $m = 1.5$ and $\beta = 1$. Therefore, a possible correlation for (K_p) will be

$$K_p = a\frac{(K_s)^{n-0.5}}{(K_{tow})^{n-1.5}}\left(1+\frac{1}{\alpha}\left(\frac{K_s}{K_{tow}}\right)^{1.5-n}\right) = K_s\left(1+\alpha\left(\frac{K_s}{K_{tow}}\right)^{n-1.5}\right) \tag{7}$$

or in terms of the dimensionless quantity $Y = K_p K_s^{1/2}(K_{tow})^{3/2}$

$$Y \equiv \frac{K_p K_s^{0.5}}{K_{tow}^{1.5}} = a\left(\frac{K_s}{K_{tow}}\right)^{n}\left(1+\frac{1}{\alpha}\left(\frac{K_s}{K_{tow}}\right)^{1.5-n}\right) \tag{8}$$

The asymptotes of (8) are:

- for large (K_s/K_{tow}), $Y \to \left(\frac{K_s}{K_{tow}}\right)^{1.5}$.

This is a line of slope 1.5 on a $\log(Y)$ vs. $\log(K_s/K_{tow})$ graph

- for small (K_s/K_{tow}), $Y \to \alpha\left(\frac{K_s}{K_{tow}}\right)^{n}$.

This is a line of slope (n) on a $\log(Y)$ vs. $\log(K_s/K_{tow})$ graph.

In terms of the "intrinsic permeability" $K_{in} = [(K_p/K_s) - 1]$ (8) can be expressed as

$$K_{in} \equiv \frac{K_p}{K_s} - 1 = \alpha\left(\frac{K_s}{K_{tow}}\right)^{n-1.5}, \tag{9}$$

which is a line of intercept $(\log(\alpha))$ and slope $(n - 1.5)$ on a $\log(K_{in})$ vs. $\log(K_s/K_{tow})$ graph. In this sense, the proposed correlation can be seen as a generalization of the correlation proposed in Papathanasiou (1997):

$$K_{in} \equiv \frac{K_p}{K_s} - 1 = \alpha(\phi_i)\left(1-\frac{1-\phi_t}{1-\phi_{max}}\right)^{\beta(\phi_i)} \tag{10}$$

in which $\alpha(\phi_i)$ and $\beta(\phi_i)$ were determined by fitting a limited number of numerical results for (K_p) corresponding to the square–square geometry. Based on a much more extensive set of computations for the more realistic hexagonal inter- and intra-tow structural arrangements, the present study has resulted in a general model for K_{in} for the more realistic case of hexagonal arrangement of bundles and for both hexagonal and square intra-tow packings. The ability of the proposed model (8) to fit the numerical data is investigated next.

3.3. Fitting the numerical results to (8)

Fig. 5 shows the results of Fig. 3 (HH array) plotted as suggested by (8). It can be seen that the numerical data collapse on a curve described by (8) with $\alpha = 3$ and $n = 0.625$. As anticipated, at very high values of (K_s/K_{tow}) (that is, for a practically impermeable tow) the numerical data approach an asymptote with a slope of 1.5 on the log–log graph. It should be noted that the values for the parameters (n) and (α) (in (8)) obtained by fitting the data of Fig. 3 are influenced by the choice of the model used to calculate K_s and K_{tow}. Gebart's model (Gebart, 1992), given by

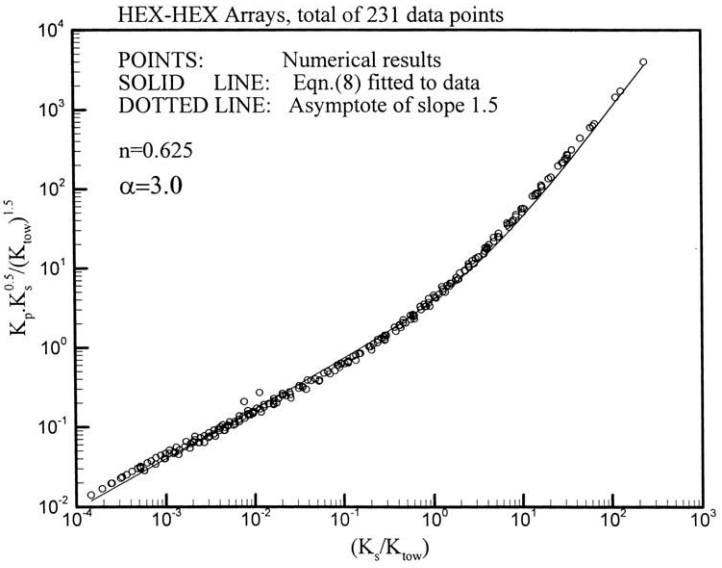

Fig. 5. Numerical results for the permeability (K_p) of HH arrays plotted on a log–log scale as suggested by Eq. (8).

$$K = \frac{16}{9\pi\sqrt{2}} \left[\sqrt{\frac{1-\phi_{\max}}{1-\phi}} - 1 \right]^{2.5} R^2 \tag{11}$$

has been used in this work. This is a well-tested model and simple to evaluate. In (11) (K) is the dimensional permeability, (ϕ) is the porosity, R the fiber radius and $\phi_{\max}$ the porosity at maximum packing. To calculate K_s we set $\phi = \phi_i$ and $R = R_{tow}$. To calculate K_{tow} we use $R = R_f$ and $\phi = \phi_t$. $\phi_{\max}$ depends on the type of packing (it is $\phi_{\max} = 1 - (\pi/2\sqrt{3})$ for hexagonal and $\phi_{\max} = 1 - \pi/4$ for square packing). It is known that (11) is strictly valid in the limit of low porosity (limit of validity of the lubrication approximation). However, (11) has been found to be in reasonable agreement with numerical calculations in single-fiber unit cells for a porosity up to 60%. Use of (11) for larger porosities does not mean that this model is used in an inappropriate range of porosities. Instead, the K_s and K_{tow} used in (8) should be seen simply as functions of ϕ_i, ϕ_t, R_f, R_t and of the type of packing (expressed through the choice of $\phi_{\max}$). Use of different expressions for K_s and K_{tow} will probably affect the values of parameters (α) and (n) determined by fitting the data of Fig. 3 to (8). Alternatively, one could use values for K_s and K_{tow} obtained numerically from single-fiber unit cells at the appropriate level of porosity and corresponding to R_{tow} (for K_s) and R_f (for K_{tow}). In this work (11) has been used for hexagonal fiber packing. For square packing it has been found that (11) is not in good agreement with the numerical results for $\phi > 0.6$. In this case, we use Eq. (11) for $\phi < 0.6$, while for $\phi > 0.6$ we apply the model proposed by Bruschke and Advani (1993), which reads

$$K = \frac{1}{4(1-\phi)} \left(\ln(\sqrt{1/1-\phi}) - \frac{3}{4} + (1-\phi) - \frac{(1-\phi)^2}{4} \right) R^2.$$

The notation is as in (11). The results for the HS arrays are shown in Fig. 6. As anticipated, the HS results also observe the same asymptote of slope 1.5 at high (K_s/K_{tow}). The higher scatter

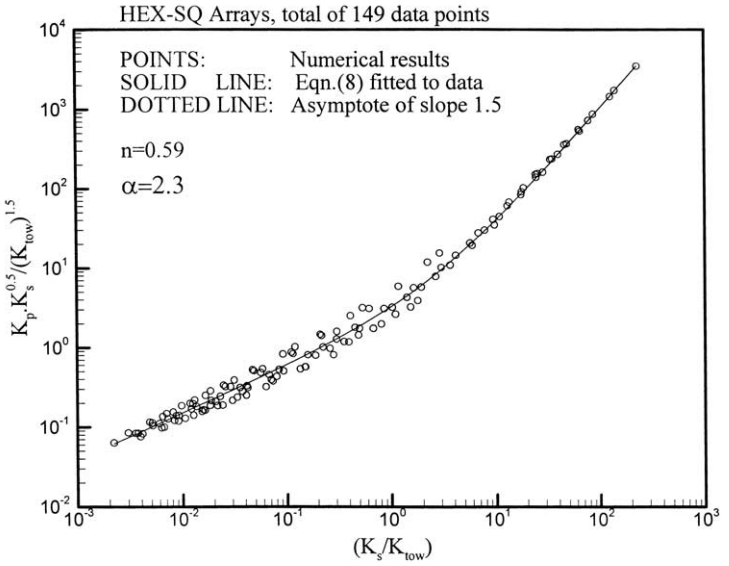

Fig. 6. Numerical results for the permeability (K_p) of HS arrays plotted on a log–log scale as suggested by Eq. (8).

observed in this case is probably due to the lower values of ϕ_i used and to the square packing of the intra-tow fibers. At low levels of ϕ_i, small changes in the location of the fibers in the perimeter of the tow tend to have a large influence on the flow resistance of the unit cell. Even though there is a small difference in the least-squares fitting parameters ($\alpha = 2.3$ and $n = 0.59$ in the HS case), it is observed that the results for both types of unit cells fall roughly on the same curve when plotted as suggested by (8). This is shown in Fig. 7, which, along with (7), suggests that the permeability of hexagonal arrays of fiber bundles can be expressed as

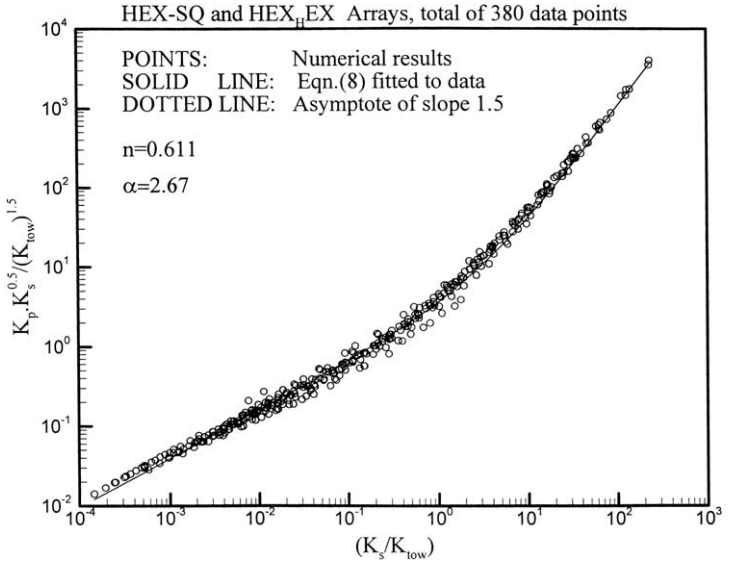

Fig. 7. Numerical results for the permeability (K_p) of HH and HS arrays plotted on a log–log scale as suggested by Eq. (8).

$$K_p = K_s \left[1 + 2.67 \left(\frac{K_{tow}}{K_s} \right)^{0.89} \right]. \tag{12}$$

K_s and K_{tow} are calculated from (11) and/or (12) as appropriate, when the porosity (ϕ), the type of packing (use (11) except for square packing and $\phi > 0.6$, in which case use (12); also use the appropriate value of ϕ_{max} in (11)) and characteristic lengths (R in (11) and (12)) are known for the inter- and the intra-tow spaces.

4. Conclusion

We presented a computational analysis of Stokes flow across hexagonal arrays of fiber bundles. Each bundle is made up of a number (up to 300) of individual filaments, arranged in either square of hexagonal packing. This approach removes all uncertainties concerning the nature of the flow within the tow or at the fluid-tow interface and allows us to consider explicitly the effect of tow microstructure on the permeability. As a result of a large number of simulations and based on earlier theoretical results we construct a master curve that describes the dependence of the permeability of a dual porosity fibrous medium on its inter- and intra-tow structures.

Acknowledgements

This work was supported by the US Department of Energy.

References

Bruschke, M.V., Advani, S.G., 1993. Flow of generalized Newtonian fluids across a periodic array of cylinders. J. Rheol. 37, 479–498.

Brebbia, C., Dominquez, J., 1992. Boundary Elements, an Introductory Course, second ed. McGraw-Hill, New York.

Darcy, H.P.G., 1856. Les Fontaines Publiques de la Ville de Dijon. Dalmont, Paris.

Drummond, J.E., Tahir, M.I., 1984. Laminar viscous flow through rectangular arrays of parallel solid cylinders. Int. J. Multiphase Flow 10, 515–540.

Gebart, B.R., 1992. Permeability of unidirectional reinforcements for RTM. J. Comp. Mater. 26, 1100–1134.

Nagelhout, D., Bhat, M.S., Heinrich, J.C., Poirier, D.R., 1995. Permeability for flow normal to a sparse array of fibers. Mater. Sci. Eng. A191, 203–208.

Papathanasiou, T.D., 1996. A structure oriented micromechanical model for viscous flow through square arrays of fiber clusters. Comp. Sci. Technol. 56, 1055–1069.

Papathanasiou, T.D., 1997. On the effective permeability of square arrays of permeable fiber tows. Int. J. Multiphase Flow 23, 81–92.

Parnas, R.S., Phelan Jr., F.R., 1991. The effect of heterogeneous porous media on mold filling in resin transfer molding. SAMPE Quart. 22, 53–60.

Phelan, F.R., Wise, G., 1996. Analysis of transverse flow in aligned fibrous porous media. Composites Part A 27A, 25–34.

Pillai, K.M., Advani, S.G., 1995. Numerical and analytical study to estimate the effect of two length scales upon the permeability of a fibrous porous medium. Transp. Porous Media 21, 1–17.

Ranganathan, S., Phelan F.R, , Advani, S.G., 1996. A generalized model for the transverse fluid permeability in unidirectional fibrous media. Polym. Compos. 17, 222–230.

Sadiq, T.A.K., Advani, S.G., Parnas, R.S., 1995. Experimental investigation of transverse flow through aligned cylinders. Int. J. Multiphase Flow 21, 755–774.

Sangani, A.G., Acrivos, A., 1982. Slow flow past periodic arrays of cylinders with applications to heat flow. Int. J. Multiphase Flow 8, 193–206.